NTU Journal for Renewable Energy (2024) Vol. 7 (1): 46 - 56
DOI: https://doi.org/10.56286/9akyr430

IRAQI Academic Scientific Journals

ISSN: 2788-9912 (print); 2788-9920 (online)
NTU Journal for Renewable Energy
Available online at:
https://journals.ntu.edu.iq/index.php/NTU-JRE

Heat Transfer and Fluid Flow Over A Bank of Longitudinally Finned Flat Tubes: A Numerical Study

Ahmed H. Ahmed[a,b,*], Maki H. Zaidan[a], Manar S.M. Al-Jethelah[a]

[a]Tikrit University /Department of Mechanical Engineering/College of Engineering /Tikrit/ Iraq

[b]Northern Technical University/ Hawija Technical Institute/ Renewable Energy Research Unit

Article Information

Received: 02 June 2024
Received in Revised form: 10 July 2024
Accepted: 22 July 2024
Published: 07 September 2024

Corresponding Author:
Ahmed H. Ahmed

Email:
ahmedhasan_hwj@ntu.edu.iq

Keywords:
Laminar forced convection;LFFTBHE; Staggered arrangements; longitudinal pitch.

ABSTRACT

This computational study investigates the heat transfer rate and fluid flow characteristics of a staggered arrangement of longitudinally finned flat tube banks ($LFFTBs$) with a constant surface temperature. The finite volume method (FVM) is used to solve the governing equations using the commercial CFD software $ANSYS\ 2021/R2$. This study considers longitudinal pitch ratios ($4 \leq \widehat{SL} \leq 5$). In addition, the dimensionless transverse pitch ratio ($\widehat{ST}$)=3 and both the dimensionless upstream fin length ratio ($\widehat{Lu}$)= ($\widehat{Ld}$) =0.8 is the dimensionless fin angle ($\widehat{\theta}$) = 0.52. The focus of the investigation is a Reynolds number range between $200 \leq Re \leq 1000$ with constant physical properties. The analysis examines pressure drop, dimensionless heat transfer rate, and the average Nusselt number. Results indicate that as Reynolds numbers increase and dimensionless longitudinal pitch ratios decrease, the heat transfer rate between tube surfaces and airflow increases to reach maximum value of 275. In addition, the Reynolds number affects the pressure drop, Began number, average Nusselt number, and thermal hydraulic performance.

1. Introduction

Heat exchangers have become an essential part of our modern commercial, industrial, and technological age, and there are as many different types of heat exchangers as available processes or applications. A particular category of heat exchangers, tube-fin heat exchangers, includes various heat exchangers to suit different applications. Air conditioners for comfort purposes, large-scale industrial and chemical processes, compact micro heat exchangers used in the aerospace or space industries, and other similar devices are some examples. Researchers are constantly developing compact and effective thermal transport systems to reduce energy consumption [1]. Industries use heat exchangers of the tubular type, including plate heat exchangers, shell and tube heat exchangers, and double pipe heat exchangers [2]. The tubular heat exchangers are relatively maintenance-free and have a modular design. However, a preliminary study by [3]. Most industrial process heat exchangers use flow over the surface of the tube or cylinder [4]. The crossflow heat exchanger is one of the many tubular heat exchangers utilized in the industry [5]. Research typically focuses on developing methodologies that maximize heat transfer while minimizing pressure drop. These innovations introduce the forced flow of a fluid, like air, over a heated surface. The heated surface could be stationary, moving, or even a combination, depending on the applications. By modifying the boundary layer and vortex formation, these techniques significantly changed the thermal and fluid flow fields and increased the convective rate of heat transfer. Recent developments include the insertion of vortex generators [6] and surface modification [7, 8]. It is worthwhile to briefly overview various studies that have looked at flow over various shapes under different flow conditions. For a long time, fluid mechanics research has been wildly attracted to the effect of flow past bluff bodies, particularly cylinders. The majority of these studies focused on flow over a cylinder. Crossflow through rigid tube bundles can be predicted numerically using a pressure drop coefficient and heat transfer coefficient. The finite-element Galerkin method is used in the scheme. Laminar steady-state flow conservation equations are formulated in terms of function and the formation of vortices. Up to a Reynolds number value of 1,000, Chang's numerical predictions and the experimental data agree well [9-11]. The heat transfer and fluid flow over a row of in-line cylinders sandwiched between two parallel plates are studied [12, 13]. The pressure drop and heat transfer were generally spatially periodic, indicating that periodically fully developed characteristics were present.

Using the finite-element method, a fluid flow over a collection of diamond-shaped fins is investigated [14], and calculated the flow and conjugate heat transfer for a thermally and hydrodynamically developing three-dimensional laminar flow in a high-performance finned oval tube heat exchanger

element [14, 15]. Two completely different numerical techniques, the lattice-Boltzmann automata (LBA) method and the finite-volume method (FVM), were used to thoroughly examine the confined flow around a square-sectioned cylinder mounted inside a plane channel. The incompressible Navier-Stokes solver for any nonorthogonal, body-fitted grid was the foundation for the finite-volume code. In addition, investigations were done on velocity profiles and critical parameters like drag coefficient, recirculation length, and Strouhal numbers [16]. The crossflow tubular heat exchangers were the most popular among the various constructional options for different thermal systems worldwide. The main driver of this widespread acceptance is the crossflow tube bank's ability to provide greater flexibility in the operating temperature and mass flow rate by varying the pitch and other geometric features. As a result, the hot fluid typically flows through the tubes while the colder fluid flows over them in tube bank installations.

The tubes are set up in an in-line configuration of well-defined square or rectangular arrays or a staggered arrangement of zigzags. The cold fluid draws the desired heat energy from the tube surface during the external flow over the tube bank. The efficiency of this energy extraction process is, therefore, greatly influenced by the fluid-flow pattern of the device. The earlier studies [17, 18]recommended various passive techniques to improve the performance of tube banks. A numerical and experimental investigation of body-fitted coordinates (BFC)-based 2-D forced convection heat transfer for staggered tube banks. The CHF with $30 \leq \mathrm{Re} \leq 200$ and $Pr = 0.71$ for ST/D of 1.25, 1.75, and 2.5. The findings demonstrate that the heat transfer rate increases as the step size and longitudinal tube diameter decrease [19]. The Reynolds number has a significant impact on the local heat transfer. Despite having fewer studies than circular-tube heat exchangers, flat-tube heat exchangers are predicted to have a lower air-side pressure drop and a higher air-side heat transfer rate. Due to a smaller wake area, the pressure drop is anticipated to be lower than for circular tubes. For the same reason, flat-tube heat exchangers are expected to have lower vibration and noise levels than circular-tube heat exchangers. These factors cause the heat exchanger's size to be reduced, which lowers losses and costs. The primary goal of this article is to investigate numerically the $2-D$ laminar incompressible flow and heat transfer over staggered configurations of longitudinally finned flat tubes.

2. THEORY

The physical model of a staggered finned flat tube bank (SLFFTBHE), as depicted in Figure 1, has been considered to improve heat transmission on the air side. Typically, this form of heat exchanger consists of multiple $SLFFTBHE$ units. The analysis assumes laminar, steady-state flow with incompressible fluid and negligible viscous dissipation. The surface temperature remains constant, and Table 1 lists the thermophysical properties of the working fluid. Figure 1 depicts the physical representation of the present problem, in which forced convection heat transfer occurs between the heated flat tube surface and the incoming airflow in a horizontal $x-y$ plane. The two-dimensional

governing equations can be summarized as follows [20]:

$$\frac{\partial u}{\partial x}+\frac{\partial v}{\partial y}=0, \quad (1)$$

$$\rho\left(u\frac{\partial u}{\partial x}+v\frac{\partial u}{\partial y}\right)=-\frac{\partial p}{\partial x}+\mu\left(\frac{\partial^2 u}{\partial x^2}+\frac{\partial^2 u}{\partial y^2}\right), \quad (2)$$

$$\rho\left(u\frac{\partial v}{\partial x}+v\frac{\partial v}{\partial y}\right)=-\frac{\partial p}{\partial y}+\mu\left(\frac{\partial^2 v}{\partial x^2}+\frac{\partial^2 v}{\partial y^2}\right) \quad (3)$$

$$\left(u\frac{\partial t}{\partial x}+v\frac{\partial t}{\partial y}\right)=\alpha\left(\frac{\partial^2 t}{\partial x^2}+\frac{\partial^2 t}{\partial y^2}\right) \quad (4)$$

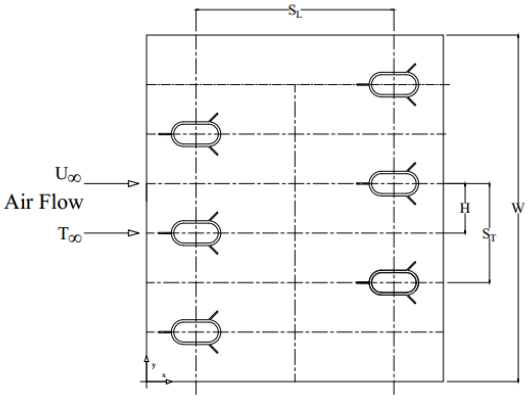

Figure 1. Rows of SLFFTB in crossflow.

To normalized Equations (1)–(4), the coordinates (x, y) are scaled by the finned tube diameter (dt), the velocities (u, v) are scaled by Δp/ρ, Δp scales the pressure (p), and the temperature (t) is risen by ($t_w - t_\infty$). Equations (1) to (4) can be non-dimensionalized by using the following dimensionless coordinates, velocities, pressure, and temperature:

$$X,Y=\frac{x,y}{Dt},\ U,V=\frac{u,v}{(\Delta p/\rho)^{\frac{1}{2}}},\ P=\frac{p}{p_{in}-p_{out}},$$

$$\theta=\frac{t-t_o}{t_w-t_o},\ Be=\frac{\Delta p \mathrm{Dt}^2}{\mu\alpha},\ Pr=\frac{\mu Cp}{K},$$

$$\widehat{ST}=\frac{ST}{DT},\widehat{Lu}=\frac{Lu}{DT},\widehat{Ld}=\frac{Ld}{DT},\widehat{SL}=\frac{SL}{DT}\ \ \hat{\theta}=\frac{\theta\,\pi}{180} \quad (5)$$

Now, with the above dimensionless variables in eq. (5), eqs. (1 –4) becomes:

$$\frac{\partial U}{\partial X}+\frac{\partial V}{\partial Y}=0, \quad (6)$$

$$U\frac{\partial U}{\partial X}+V\frac{\partial U}{\partial Y}=-\frac{\partial P}{\partial X}+\sqrt{\frac{Pr}{Be}}\left(\frac{\partial^2 U}{\partial X^2}+\frac{\partial^2 U}{\partial Y^2}\right) \quad (7)$$

$$U\frac{\partial V}{\partial X}+V\frac{\partial V}{\partial Y}=-\frac{\partial P}{\partial X}+\sqrt{\frac{Pr}{Be}}\left(\frac{\partial^2 V}{\partial X^2}+\frac{\partial^2 V}{\partial Y^2}\right) \quad (8)$$

$$U\frac{\partial \theta}{\partial X}+V\frac{\partial \theta}{\partial Y}=\frac{1}{\sqrt{(\mathrm{BePr})}}\left(\frac{\partial^2 \theta}{\partial X^2}+\frac{\partial^2 \theta}{\partial Y^2}\right) \quad (9)$$

The another dimensionlles are dominated by heat transfer and fluid flow:

$$\mathrm{Nu}=(hd)/K,\ \mathrm{qds}=\frac{\mathrm{Qt}}{\mathrm{K(Ts-Tb)}}\ \ Re=\frac{\rho \mathrm{VD}}{\mathrm{K}\mu} \quad (10)$$

The schematic of staggered tube banks and the computational domain is shown in 'figure 1'. Boundary conditions are as follows:

$$(A): U=V=0,\theta=1 \quad (11)$$

$$(B): \frac{\partial U}{\partial Y}=0,V=0,\frac{\partial \theta}{\partial Y}=0 \quad (12)$$

$$(I): U=1,\frac{\partial V}{\partial X}=0,\theta=0 \quad (13)$$

$$(E): \frac{\partial U}{\partial X}=\frac{\partial V}{\partial X}=0,\frac{\partial \theta}{\partial X}=0 \quad (14)$$

Eq. (7) was solved numerically using a control volume-based finite volume method (Fluent-CFD) software solver. The grid is made up of triangular elements, using a SIMPLE procedure.

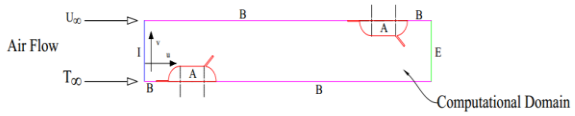

Figure 2. Boundary Conditions for (U, V, P, and θ) around and on LFFTB in crossflow.

Table 1. Thermo physical properties of the working fluid.

Physical Properties	Symbol	Values	Unit
Density	ρ	1.2245	kg/m^3
Thermal Diffusivity	α	2.2184×10^{-5}	$m^2 * s\hat{} - 1$
Thermal Conductivity	k	0.0254	$w/m℃$
Prandtl Number	pr	0.7108	–
Specific Heat	Cp	1005	$kj/kg℃$
Dynamic Viscosity	μ	1.797E-05	kg/ms

3. VALIDATION

For the Longitudinally Finned Flat Tube Bank ($LFFTB$), simulations were performed under steady-state conditions. Using the same reference, Figure 3 validates the $LFFTB's$ configuration in a staggered arrangement. In Figure 4, the average Nusselt number concerning Reynolds number at a Prandtl number (Pr) of 0.7, a transverse pitch ratio ($\widehat{ST}$) of 3.0, and a longitudinal pitch ratio ($\widehat{SL}$) of 4.0 is compared to previous research. The transverse element size was set to 0.0005, yielding 24,907 cells, and the Reynolds number ranged between 10 and 100. Notably, there is an impressive correlation between the present study's findings and previous numerical results [20].

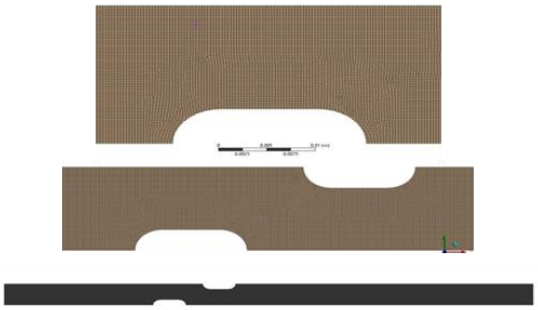

Figure 3. Schematic of grid systems generated by finite volume method made up of triangular elements.

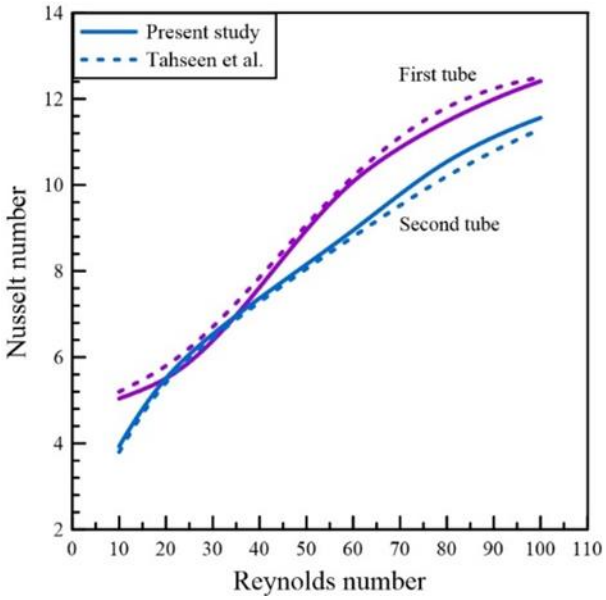

Figure 4. Comparison of Nusselt Number with Reynolds Number between the Present Study and Previous Literature [20].

4. RESULTS AND DISCUSSION

Several independent governing parameters influence the fluid flow and heat transmission over a bank of longitudinally finned flat tubes in staggered configurations.

These configurations keep the surface temperature and Prandtl number constant. Specifically, the dimensionless longitudinal pitch ratios ($\widehat{SL}$) are set to 4, 4.5, and 5 in ascending order. Dimensionless ratios for upstream fin length ($\widehat{Lu}$) and downstream fin length ($\widehat{Ld}$) are each 0.8. Moreover, the dimensionless fin angle $\hat{\theta}$=0.52 degrees, and $\widehat{ST} = 4$.

The investigation encompasses Reynolds numbers ranging from 200 to 1000, with physical properties held constant. Several parameters, such as pressure drop, dimensionless heat transfer rate, average Nusselt number, and Began number, have been investigated. The fluid's motion is undulating, and a separation zone forms behind the cylinder. Observation reveals that the fluid temperature is lower at the inlet and progressively increases as it reaches the surface of the hot tube. Along the surface facing upstream, temperature contours diffuse downstream as they are densely packed. Particularly near the separation point, a relatively thick thermal layer is observed in the separation zone. As Reynolds numbers increase, the isotherms with lower values penetrate deeply, bringing colder fluid closer to the heated surface. This behavior increases heat transfer. The velocity and temperature contours for each of the three longitudinal pitches are shown in Figures 5 and 6, respectively.

The distribution of velocity and temperature are highly correlated. Depending on the fluid's speed, the fluid exits the test area at a higher temperature, as the temperature rises from the lowest possible at entry, which is the ambient temperature, to the highest temperature in the contact area at the hot tube's surface. The following will explain how heat transfer works. The effect of the Reynolds number can be distinguished clearly by looking at the velocity contour because the fluid has the lowest velocity when it enters the test area. Vortices behind the fins and reverse flow also occur during this process, which is a good enough explanation to explain why heat transfer will improve in the future.

The relationship between the dimensionless longitudinal pitch ratio and the non-dimensional heat transfer rate is depicted in Figure 7. In light of the previous sentence, it is obvious why the heat transfer rate has increased to reach maximum value of 310. The behavior of the heat transfer rate can be adequately explained by the occurrence of vortices in the vicinity of the fins' surfaces and the increase in speed, which is consistent with.

The relationship between the dimensionless longitudinal pitch ratio and the dimensionless pressure drop is shown in Figure 8. The reader will initially assume that the Reynolds number and the dimensionless pressure drop have an inverse relationship to reach maximum value of 9.7. This is true when the connection is with the pressure difference itself because, to translate pressure into dimensions, one must divide by the square of the velocity, which inverts the relationship.

In contrast, the relationship with the Reynolds number is inverse, while the relationship with the angle of deviation of the fins is not. The relationship between the Nusselt number and the dimensionless longitudinal pitch ratios for various Reynolds number is shown in Figure 9. One of the main

issues for researchers in this field is the thermal resistance at the air side of heat exchangers. Since the air side has few physical characteristics compared to the fluid resistance, which is almost nonexistent, the heat exchanger's designer is interested in the possibility of transferring the most heat there. The only restriction is the potential to create turbulent flow by raising the Reynolds number, as shown in the above figure, to improve the convection heat transfer coefficient to reach maximum value of the Nusselt number of 9.5 constrict to the high Reynolds number for various dimensionless longitudinal pitch ratios.

The relationship between Bejan's number and the dimensionless longitudinal pitch ratios for various the Reynolds number is shown in Figures 10. The dimensionless pressure drop and Bejan number are closely related, but Bejan number ultimately determines the pressure drop. which is a direct relationship between the two quantities. This is because an increase in the dimensionless longitudinal pitch ratio increases the flow area and a corresponding decrease in the Reynolds number.

The relation between dimensionless thermal hydraulic performance against dimensionless longitudinal pitch for various Reynolds number is direct proportionality. The above explanation can be considered sufficient for the relationship between the friction factor and the Claiborne factor refers to the friction resulting from the movement of the fluid, so, logically, any increase in the Reynolds number is accompanied by an increase in friction Figure 11.

The primary goal of the design is to increase the coefficient of heat transfer by convection, provided that the pressure drop is considered. However, the pressure drop is less than 50 pa based on the results. When the corresponding pumping power is calculated, it is almost insignificant compared to the amount of heat transfer by the air.

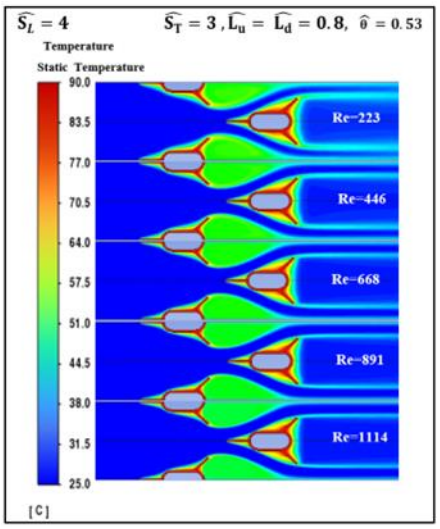

(a)

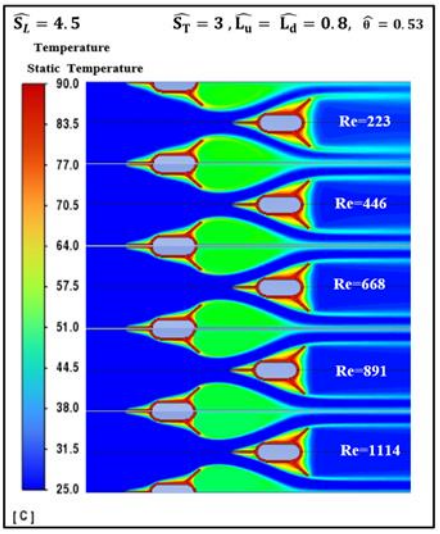

(b)

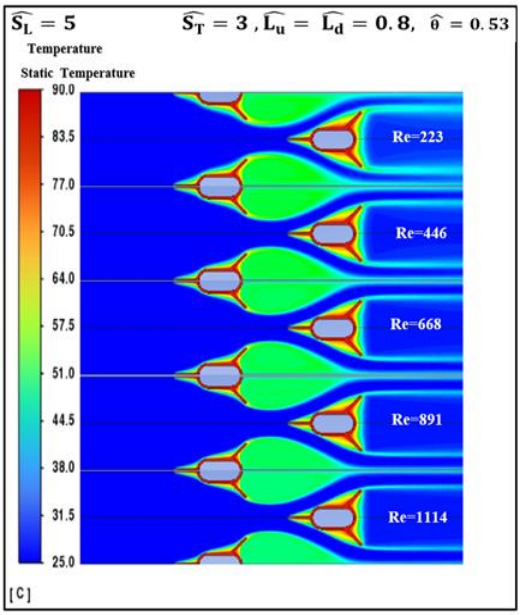

(c)

Figure 5. (a, b & c) Temperature contour for different $\widehat{SL}$with $\widehat{Ld}$=0.8, $\widehat{ST}$=3, $\widehat{Lu}$=0.8, $\hat{\theta} = 0.53$, and $200 \leq \text{Re} \leq 1000$.

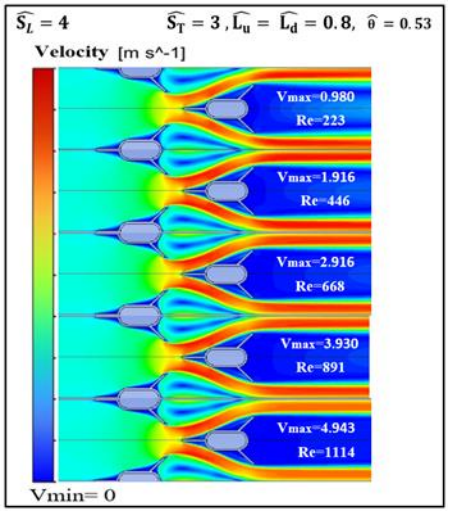

(a)

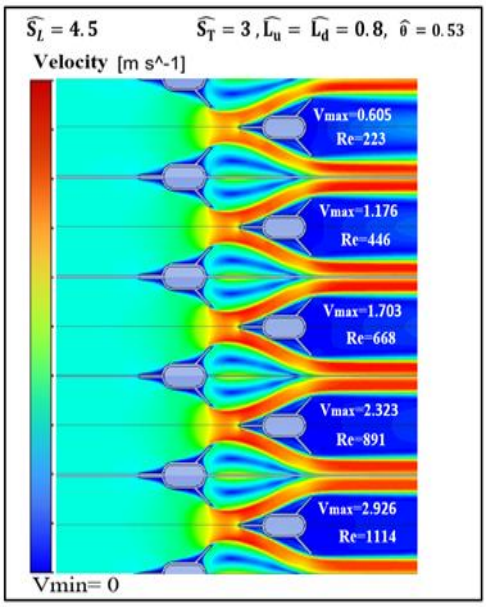

(b)

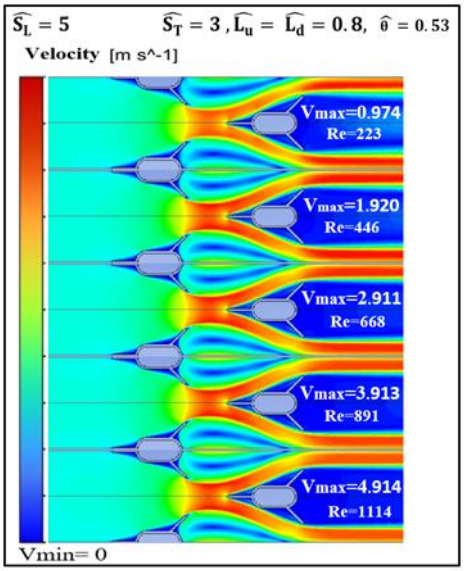

(c)

Figure 6. (a, b & c) Velocity contour for different $\widehat{SL}$with $\widehat{Ld}$=0.8, $\widehat{ST}$=3, $\widehat{Lu}$=0.8, $\hat{\theta} = 0.53$, and $200 \leq \text{Re} \leq 1000$.

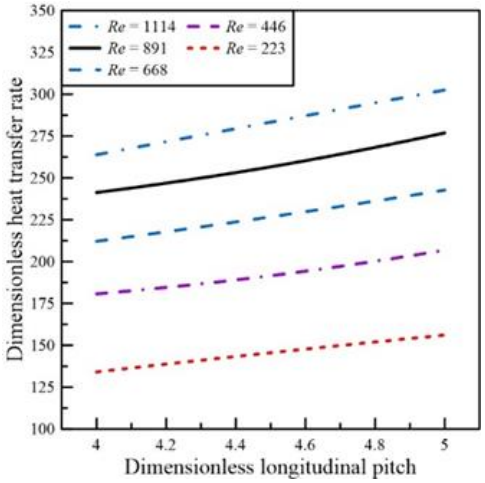

Figure 7. Dimensionless overall heat transfer rate against dimensionless longitudinal pitch for various Reynolds numbers.

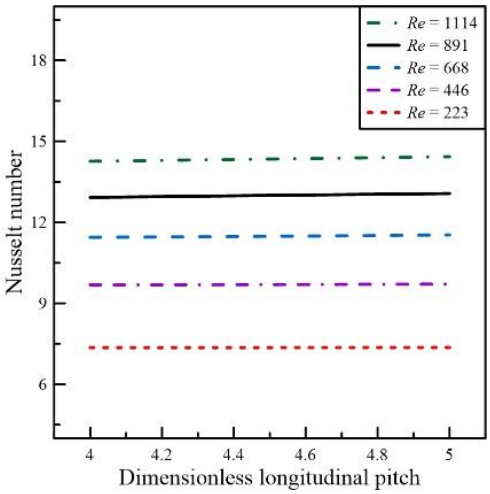

Figure 9. Dimensionless Nusselt number against dimensionless longitudinal pitches for various Reynolds number.

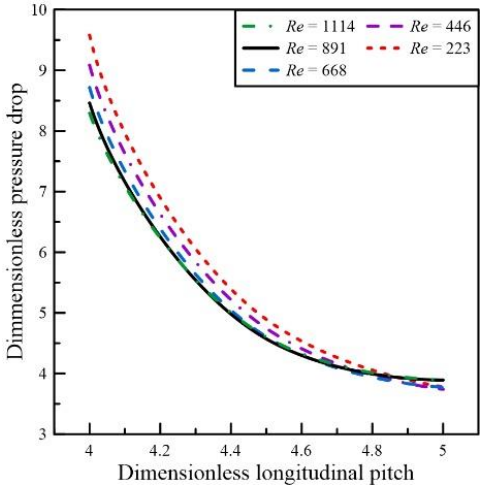

Figure 8. Dimensionless pressure drop against dimensionless longitudinal pitch for various Reynolds number.

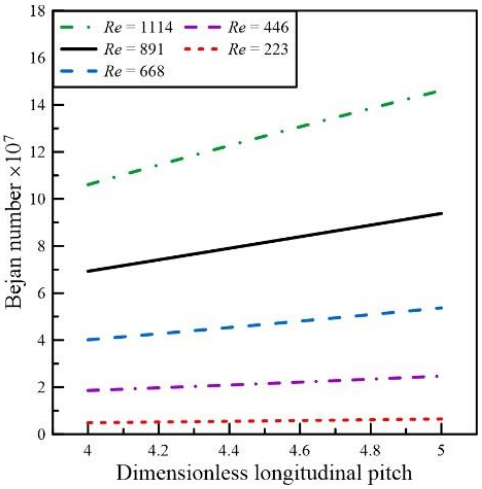

Figure 10. Influence of Bejan number on the dimensionless longitudinal pitch for various Reynolds numbers.

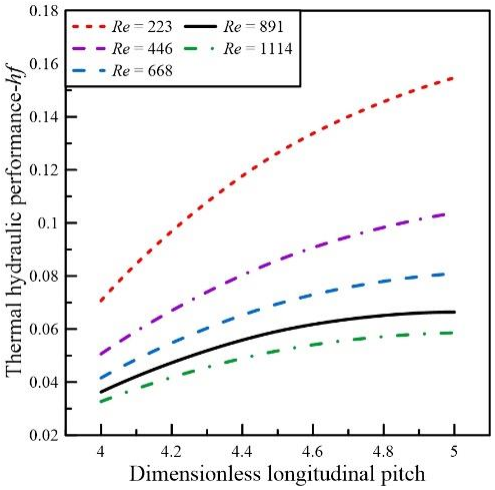

Figure 11. Dimensionless thermal hydraulic performance against dimensionless longitudinal pitch for various Reynolds number.

CONCLUSION

The numerical results of temperature distributions, the streamlining of airflow, and the average Nusselt number were studied. It is observed that:

- The Began number is increasing, and the Reynolds numbers are increasing for any longitudinal pitch.
- The pressure drop is decreased, and the Reynolds numbers are increased for longitudinal pitch less than 5.
- The isothermal floods decrease with the increase in Reynolds numbers the flow recirculation region increases with the increase in Reynolds number. The average Nusselt number of air flow increases with the increase of the Reynolds number.

Finally, longitudinal pitch increases and the average Nusselt number decreases for any Reynolds number.

ACKNOWLEDGEMENTS

The authors thank the Faculty of Mechanical Engineering at Tikrit University and Northern Technical University, Technical Institute, Renewable Energy Research Unit, Hawija, Iraq.

REFERENCES:

[1] Shah, R.K. and D.P. Sekulic, *Fundamentals of heat exchanger design*. 2003: John Wiley & Sons.

[2] Ganapathy, V., *Industrial boilers and heat recovery steam generators: design, applications, and calculations*. 2002: CRC Press.

[3] Bejan, A., *Convection heat transfer*. 2013: John wiley & sons.

[4] Sumner, D., et al., *Fluid behaviour of side-by-side circular cylinders in steady cross-flow.* Journal of Fluids and Structures, 1999. **13**(3): p. 309-338.

[5] Tahseen, T.A., M. Ishak, and M.M. Rahman, *An overview on thermal and fluid flow characteristics in a plain plate finned and un-finned tube banks heat exchanger.* Renewable and Sustainable Energy Reviews, 2015. **43**: p. 363-380.

[6] Samadifar, M. and D. Toghraie, *Numerical simulation of heat transfer enhancement in a plate-fin heat exchanger using a new type of vortex generators.* Applied Thermal Engineering, 2018. **133**: p. 671-681.

[7] Liu, S. and M. Sakr, *A comprehensive review on passive heat transfer enhancements in pipe exchangers.* Renewable and sustainable energy reviews, 2013. **19**: p. 64-81.

[8]Williamson, C.H.K., *Vortex dynamics in the cylinder wake.* Annual review of fluid mechanics, 1996. **28**(1): p. 477-539.
[9] Hoftyzer, M. and E. Dragomirescu. *Numerical investigation of flow behaviour around inclined circular cylinders*.
[10] Chang, Y., A.N. Beris, and E.E. Michaelides, *A numerical study of heat and momentum transfer for tube bundles in crossflow*. International journal for numerical methods in fluids, 1989. **9**(11): p. 1381-1394.
[11] Kundu, D., A. Haji-Sheikh, and D.Y.S. Lou, *Heat transfer predictions in cross flow over cylinders between two parallel plates.* Numerical Heat Transfer, 1991. **19**(3): p. 361-377.
[12] Kundu, D., A. Haji-Sheikh, and D.Y.S. Lou, *Heat transfer in crossflow over cylinders between two parallel plates.* 1992.
[13] Grannis, V.B. and E.M. Sparrow, *Numerical simulation of fluid flow through an array of diamond-shaped pin fins.* Numerical Heat Transfer, 1991. **19**(4): p. 381-403.
[14] Chen, Y., M. Fiebig, and N.K. Mitra, *Conjugate heat transfer of a finned oval tube part A: flow patterns.* Numerical Heat Transfer, Part A Applications, 1998. **33**(4): p. 371-385.
[15] Breuer, M., et al., *Accurate computations of the laminar flow past a square cylinder based on two different methods: lattice-Boltzmann and finite-volume.* International journal of heat and fluid flow, 2000. **21**(2): p. 186-196.
[16] Bhuiyan, A.A. and A.K.M.S. Islam, *Thermal and hydraulic performance of finned-tube heat exchangers under different flow ranges: A review on modeling and experiment.* International Journal of Heat and Mass Transfer, 2016. **101**: p. 38-59.
[17] Wang, P., et al., *An investigation of influence factor including different tube bundles on inclined elliptical fin-tube heat exchanger.* International Journal of Heat and Mass Transfer, 2019. **142**: p. 118448.
[18] Tahseen, T.A., M.M. Rahman, and M. Ishak, *An experimental study of air flow and heat transfer over in–line flat tube bank.* International Journal of Automotive and Mechanical Engineering, 2014. **9**: p. 1487-1500.
[19] Ferziger, J.H., M. Perić, and R.L. Street, *Computational methods for fluid dynamics*. 2019: springer.
[20] Tahseen, T.A., M. Ishak, and M.M. Rahman, *Analysis of laminar forced convection of air for crossflow over two staggered flat tubes.* International Journal of Automotive and Mechanical Engineering, 2012. **6**: p. 755-767.